

HUBBLE SPACE TELESCOPE OBSERVATIONS OF THE OLDEST STAR CLUSTERS IN THE LMC

JENNIFER A. JOHNSON¹, MICHAEL BOLTE

UCO/Lick Observatory, University of California, Santa Cruz, CA 95064; jennifer@ucolick.org, bolte@ucolick.org

PETER B. STETSON, JAMES E. HESSER

Dominion Astrophysical Observatory, Herzberg Institute of Astrophysics, National Research Council of Canada, 5071 West
Saanich Road, Victoria, BC V8X 4M6, Canada; firstname.lastname@hia.nrc.ca

RACHEL S. SOMERVILLE

Racah Institute of Physics, The Hebrew University, Jerusalem, 91904, Israel; rachels@astro.huji.ac.il

ABSTRACT

We present V , $V-I$ color-magnitude diagrams (CMDs) for three old star clusters in the Large Magellanic Cloud (LMC): NGC 1466, NGC 2257 and Hodge 11. Our data extend ~ 3 magnitudes below the main-sequence turnoff, allowing us to determine accurate relative ages and the blue straggler frequencies. Based on a differential comparison of the CMDs, any age difference between the three LMC clusters is less than 1.5 Gyr. Comparing their CMDs to those of M 92 and M 3, the LMC clusters, unless their published metallicities are significantly in error, are the same age as the old Galactic globulars. The similar ages to Galactic globulars are shown to be consistent with hierarchical clustering models of galaxy formation. The blue straggler frequencies are also similar to those of Galactic globular clusters. We derive a true distance modulus to the LMC of $(m-M)_0 = 18.46 \pm 0.09$ (assuming $(m-M)_0 = 14.61$ for M 92) using these three LMC clusters.

Subject headings: blue stragglers — globular clusters: individual (NGC 1466, NGC 2257, Hodge 11) — Magellanic Clouds

1. INTRODUCTION

Only in the Magellanic Clouds and the Milky Way Galaxy can we *directly* measure the ages of old star clusters and thereby accurately model the history of cluster formation. In the Galaxy, after decades of research into dating techniques and collecting data for halo globular clusters (including, very recently, globulars in the far reaches of the halo using the Hubble Space Telescope and WFPC2 (e.g., Harris *et al.* 1997; Stetson *et al.* 1999)), we are beginning to understand the details of the cluster age distribution. As this story unfolds, a next step is to compare the early formation history of the Galaxy with that inferred from the same measurement techniques for star clusters in the Magellanic Clouds.

The most important questions to ask are (1) whether the oldest Large Magellanic Cloud (LMC) clusters are as old as the oldest Galactic globular clusters (GGCs), and (2) whether there is an age spread among the most metal-poor LMC clusters. The answer to the first question tells us about the epoch of initial cluster formation for galaxies of different mass and Hubble type. The age spread among the old clusters is one tracer of the early star formation history of the galaxy, and indicates timescales important for collapsing or merging gas clouds. Although the complete age distribution of the GGCs is not yet known, the evidence to date suggests that the majority of the Milky Way's halo clusters formed at the same time, with a small fraction of clusters that formed up to ~ 4 Gyrs later (Stetson, VandenBerg & Bolte 1996; although see Sarajedini, Chaboyer & Demarque 1997 for a different view). What fraction of the co-eval clusters formed in a single parent body or in smaller structures that later merged is not clear. The present results for the LMC also suggest a mostly co-eval population of old clusters (Brocato *et al.* 1996; Olsen *et al.* 1998).

The first studies to attempt to measure ages for the old clusters in the LMC appeared in the mid 1980s. Studies of Hodge 11 (Stryker *et al.* 1984; Andersen, Blecha, & Walker 1984), NGC 2257 (Stryker 1983; Hesser *et al.* 1984), and several clusters in the series of articles by Walker (referenced in Walker, 1993) led the way in studies of these sorts. However the combination of large distance to the LMC and problems with field-star contamination made even relative age determinations with precision of a few Gyr or better difficult. Because of the superb resolution of the Hubble Space Telescope (HST), color-magnitude diagrams (CMDs) can now be measured in the cluster cores, which substantially reduces the impact of field star contamination. With a modest effort using HST, stars three to four magnitudes below the main-sequence turnoff can be measured with good accuracy.

We have WFPC2 images in F555W and F814W of seven old LMC clusters selected to have RR Lyrae stars or very blue horizontal-branch morphology (see Table 1). In this paper we present color-magnitude diagrams for NGC 1466, NGC 2257 and Hodge 11, estimate their ages relative to GGCs, and determine their blue straggler specific frequencies.

2. OBSERVATIONS AND DATA REDUCTION

All of our clusters were observed in Cycle 5.¹ Each cluster was imaged for 2 x 260s and 3 x 1000s in F555W (\sim Johnson V) and 2 x 260s and 4 x 1000s in F814W (\sim Cousins I). The exposures were dithered to reduce the effect of undersampling which is aggravated by subpixel quantum-efficiency variations. For NGC 1466, the cluster was centered on the PC. Both NGC 2257 and Hodge 11 were centered on WF3. Figures 1a – c show the mosaicked images of our three clusters.

For our final reduction, we obtained recalibrated images from

¹Guest User, Canadian Astronomy Data Centre, which is operated by the Herzberg Institute of Astrophysics, National Research Council of Canada.

¹Bolte, P.I. Proposal Number 05897

TABLE 1
LMC CLUSTER DATA

Cluster	[Fe/H]	M_V	Proj. Radius	RR Lyrae?
Hodge 11	-2.06	-6.99	4.7°	no
NGC 1466	-1.85	-7.89	8.4°	yes
NGC 1841	-2.11	-7.86	8.4°	yes
NGC 1786	-1.87	-7.88	2.5°	?
NGC 2210	-1.97	-8.09	4.4°	yes
NGC 2257	-1.80	-6.91	8.4°	yes
Reticulum	-1.71	-5.96	11.4°	yes

NOTE.—Data from Suntzeff *et al.* (1992)

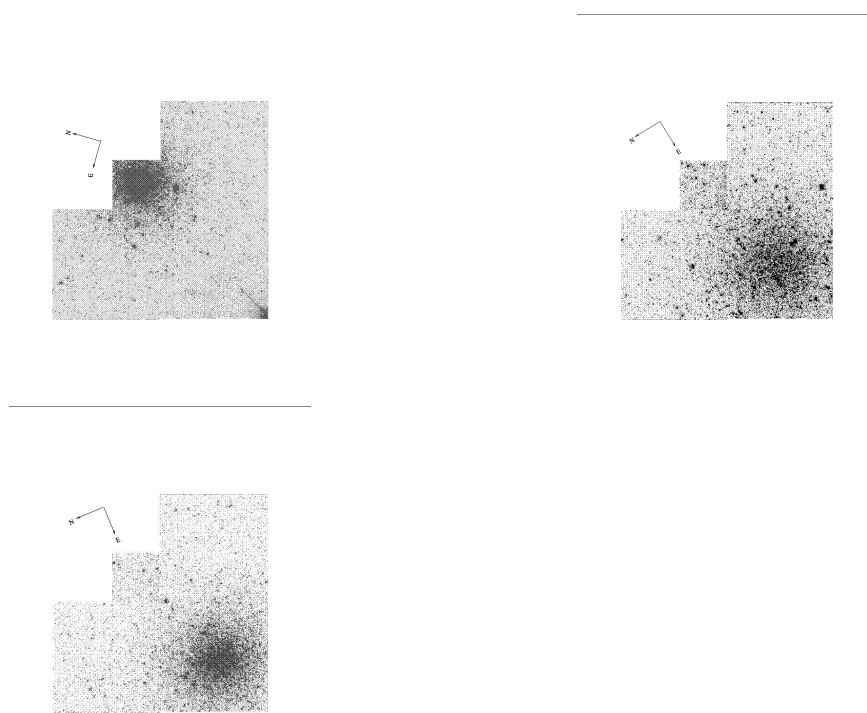


FIG. 1.—Mosaicked V -band images of the NGC 1466 WFPC2 field (top-left), the NGC 2257 WFPC2 field (top-right) and the Hodge 11 WFPC2 field (bottom-left)

the Canadian Astronomy Data Centre that had have been reduced using the most appropriate biases, darks, flats and bad-pixel masks. These calibration frames were obtained closer in time to the object frames than the ones originally used in the standard HST pipeline. We then masked the vignetted portions of the chips and corrected the pixel values for changes in effective pixel area over the chips.

For the photometry, we used the ALLSTAR/ALLFRAME suite of programs which do point-spread-function (PSF) fitting to determine magnitudes (Stetson 1987, 1992, 1994). The PSF varies spatially across each chip and temporally as the HST focus drifts. We created a PSF by combining Tiny Tim (Krist 1995) PSFs and PSFs generated by DAOPHOT from our images. A DAOPHOT PSF for the inner three pixels of the model PSF was created for each chip using the images that had the best distribution of stars on that chip. Because we lacked isolated, bright stars to determine the wings of the PSF, we used the Tiny Tim PSF beyond 3 pixels. Judging by the widths of the horizontal and red giant branches and by the lack of trends of aperture correction with position, our PSFs did a reasonable, although not perfect, job of mapping the spatial variations in the PSF. We will return to this when discussing our fiducial lines.

We set the weighting parameters “profile error” and “percent error” to zero in ALLSTAR and ALLFRAME, as suggested by Cool & King (1995). This eliminates the deviation of the pixels from the PSF and errors in the flatfielding from the weighting scheme. ALLSTAR and ALLFRAME essentially did intensity-weighted aperture photometry of the inner 1.75-2 pixels, then added a correction for the amount of light in the wings appropriate for the PSF at the star’s position.

In detail, for each cluster we ran FIND and ALLSTAR on each frame separately. Next, we matched stars between frames using DAOMASTER (Stetson 1993) only including stars on the master list which appeared on at least three frames. This successfully removed cosmic rays from the list. This master list was input into ALLFRAME which uses one star list for all frames, but determines magnitudes for each frame individually. Thus we have five measured *V* magnitudes and six *I* magnitudes for most of the objects in each cluster.

The ALLFRAME magnitudes required several corrections before we could calibrate the data using the transformation equations of Holtzman *et al.* (1995). We first needed to correct for the difference between our PSF magnitudes and apertures of 0''.5, which is the aperture size used by Holtzman *et al.* in deriving their transformation equations. To do this, we found cosmic ray hits on our images by comparing each individual image with a cosmic-ray-cleaned image created by taking the median of a registered stack of frames. Pixels in each frame which deviated by more than 2σ from the value in the medianed image were flagged and the IRAF task FIXPIX was used to interpolate over them. We next selected a set of fairly isolated stars on each frame and subtracted all other stars. Stars that had more than two flagged pixels within 0''.5 or any pixels flagged within three pixels (\sim two PSF fitting radii) of their centers were rejected. For each frame, the mean difference between the PSF and 0''.5 aperture magnitudes for the culled list of stars was determined. This value was the aperture correction and was added to all the PSF magnitudes for that frame.

For the short exposures on the PC chip for NGC 2257 and Hodge 11, the difference between aperture and PSF-based magnitudes was magnitude-dependent. This is due to the WFPC2 charge-transfer efficiency (CTE) problems, since there were not enough photons in the wings of the faint stars to fill up the

charge traps. For these two clusters the PC has only a small fraction of the total cluster stars, so we did not use it. For NGC 1466, the PC had a much higher background and the aperture corrections were constant with magnitude. We also note that we used sky annuli of 2''.0 to 2''.5, instead of the 4'' and 6'' that Holtzman *et al.* used. This reduced the effects of badly subtracted neighbors in crowded regions and uneven sky brightness across the cluster face. However, there is a difference between using the closer sky apertures and the more distant ones due to contributions from the wings of the stars. Based on our model PSFs, this difference is only 0.001 mags – much smaller than our errors in the aperture corrections (see below).

Within 0''.5, most of stars were affected by residuals from subtracted neighbors and cosmic rays. The RMS scatter in the aperture corrections (aperture – PSF magnitudes) for an individual frame ranged from ~ 0.02 to ~ 0.04 mag. To see what random errors this observational scatter introduced into our zeropoints, we used DAOMASTER to calculate the average magnitude offset for each frame among all the stars common to all frames in each filter + field combination. After accounting for the expected offset due to different exposure times, any remaining offset is a result of errors in our aperture correction. We are assuming here that the PSF of WFPC2 did not change in the amount of time it took to take images of one cluster (~ 4 hours). We fit a Gaussian to the distribution of all the offsets and found our 2σ errors to be 0.014 mags. Since DAOMASTER removes these offsets when averaging magnitudes, essentially bringing all images to the zeropoint of one frame, this is the error for our averaged magnitude zeropoints as well. We note that this error does not include any systematic error that may result if 0''.5 apertures do not include a PSF-independent fraction of the light.

After adding the aperture corrections, we corrected for the CTE problem in the *y*-direction, using the prescription of Whitmore & Heyer (1997) for 0''.5 apertures. Our PSFs are not good enough to allow accurate interpolation of saturated stars, so these stars were eliminated. We averaged our five F555W measurements and six F814W measurements using DAOMASTER and kept only the stars with errors < 0.08 mag in both filters. Finally, we calibrated the data using the Holtzman *et al.* equations. We list the photometry and positions for all our stars in Tables 2a-c. We used the first *V* exposure to determine the listed *X* and *Y* coordinates. (Tables 2a-c available from the first author)

In addition to the random errors caused by scatter in the aperture corrections (0.014 mag), there is added uncertainty from the Holtzman *et al.* zero points (~ 0.03 mag), and from the Whitmore & Heyer corrections (~ 0.02 mag) (see Stetson 1998). Adding these errors in quadrature leads to an overall error of 0.04, most of it systematic, in our zeropoints. The systematic error in *V*–*I* is more likely to be ~ 0.02 , because the uncertainties in the Whitmore & Heyer corrections and probably in the Holtzman zero points are correlated between *V* and *I*.

3. COMPARISON WITH PREVIOUS PHOTOMETRY

Each of these clusters has at least one CCD-based photometric study that we can compare with ours. Our general procedure for making comparisons was to find stars in common between our study and the previous ones and eliminate all stars from the joint sample where we detected a companion within 0''.5 in our HST images. We also exclude stars within 1 magnitude of the detection limit of the ground-based sample. In each case our

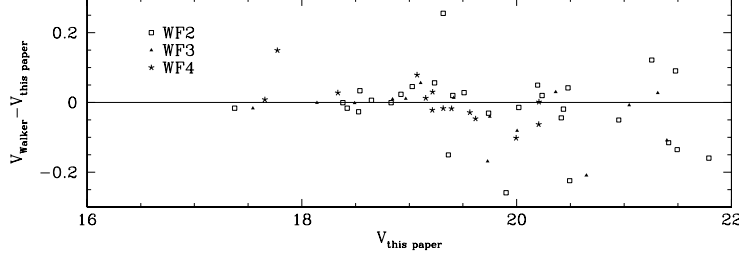


FIG. 2.— Comparison of Walker's and our photometry for NGC 1466. A line is drawn at $\Delta mag = 0$ for reference.

TABLE 3
PHOTOMETRY COMPARISONS

Cluster	Author	Chip	Filter	$Mag_{previous} - Mag_{us}$	# Stars
NGC 1466	Walker 1992b	WF2	V	-0.007 ± 0.018	32
NGC 1466	Walker 1992b	WF3	V	0.009 ± 0.020	17
NGC 1466	Walker 1992b	WF4	V	-0.008 ± 0.016	16
Hodge 11	Walker 1993	WF2	V	0.016 ± 0.011	80
Hodge 11	Walker 1993	WF4	V	0.039 ± 0.014	53
Hodge 11	Walker 1993	WF2	I	-0.007 ± 0.026	87
Hodge 11	Walker 1993	WF4	I	-0.007 ± 0.021	54
Hodge 11	Mighell <i>et al.</i> 1996	WF3	V	0.051 ± 0.005	144
Hodge 11	Mighell <i>et al.</i> 1996	WF4	V	0.032 ± 0.007	46
NGC 2257	Walker 1989	WF2	V	-0.017 ± 0.008	26
NGC 2257	Walker 1989	WF3	V	-0.027 ± 0.013	83
NGC 2257	Walker 1989	WF4	V	-0.002 ± 0.008	16
NGC 2257	Testa <i>et al.</i> 1995	WF2	V	-0.047 ± 0.008	102
NGC 2257	Testa <i>et al.</i> 1995	WF3	V	-0.012 ± 0.005	100
NGC 2257	Testa <i>et al.</i> 1995	WF4	V	-0.046 ± 0.008	109

calculated offsets and errors are tabulated in Table 3.

For NGC 1466, Walker (1992b) published B , V values for

stars with $V < 23.2$ mag and further than $13''.6$ from the cluster center. Figure 2 shows the differences between photometries

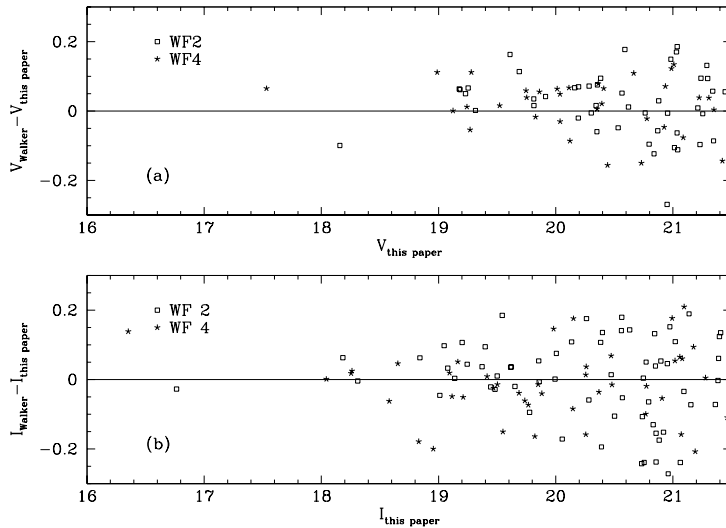


FIG. 3.— Comparison of Walker's and our photometry for Hodge 11. (a) V magnitudes (b) I magnitudes. A line is drawn at $\Delta mag = 0$ for reference.

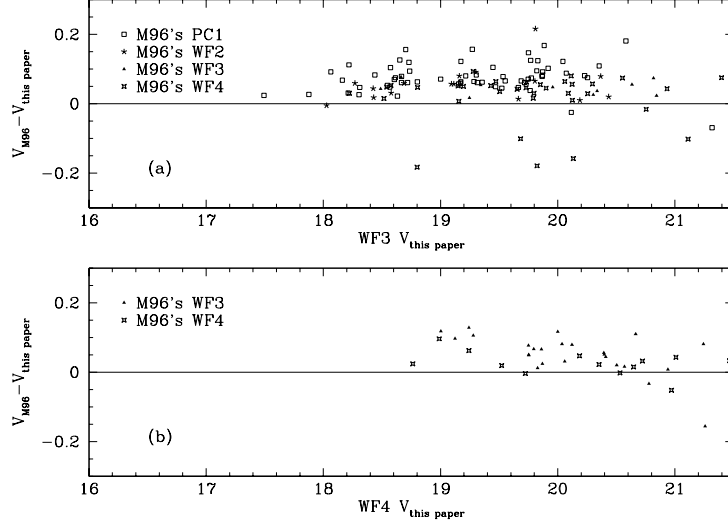


FIG. 4.— Comparison of Mighell *et al.*'s (1996) and our photometry for Hodge 11. We plot the M96 stars found on our (a) WF3 and (b) WF4. A line is drawn at $\Delta\text{mag} = 0$ for reference.

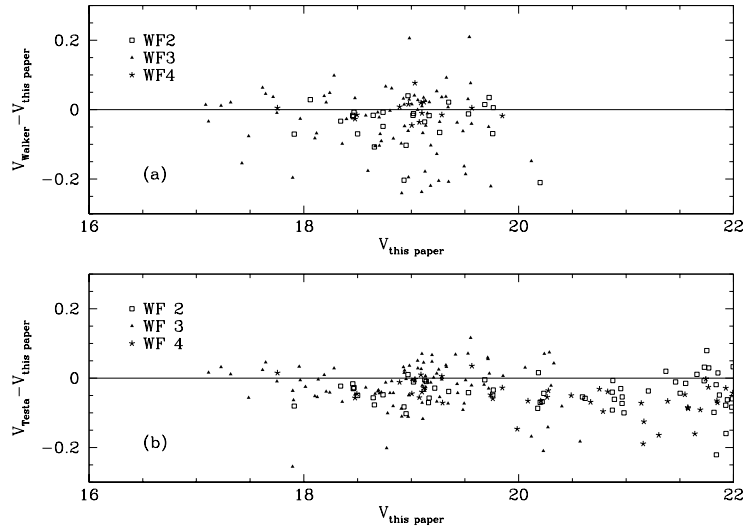


FIG. 5.— Comparison of our photometry and (a) Walker's photometry (b) Testa *et al.*'s photometry for NGC 2257. A line is drawn at $\Delta\text{mag} = 0$ for reference.

for the three WF chips. (The PC had very few stars with measurements by Walker.) The stars in common between the two studies are mostly at the faint end of Walker's study where he did not quote errors. So instead of finding a weighted mean, we found the median Δmag . Our estimate of σ comes from half of the difference between the value $> 16\%$ of the Δmags and the value $> 84\%$ of the Δmags . This estimate of σ is then reduced by square root of the number of measurements, to estimate the standard error of the mean.

For Hodge 11, Walker (1993) imaged in V and I . Because of the crowding from the ground, Walker excluded all stars closer to the cluster center than $40''$, so no stars from WF3 were included in the comparison. The V and I magnitude comparisons (Figures 3a-b) show a large scatter, but no zero-point offset or trends with magnitude. Mighell *et al.* (1996) published B , V data on Hodge 11 obtained as part of a snapshot survey of Magellanic Cloud clusters. In Figures 4a-b, we plot the difference between our WF3 and WF4 data and matching stars in the

Mighell *et al.* photometry. We calculated a weighted average of difference, using 3σ clipping.

NGC 2257 is the sparsest cluster of the three and has ground-based photometry in the cluster center. Both Walker (1989) and Testa *et al.* (1995) have B , V data. Testa *et al.* used Walker's photometry to calibrate their data, but the Testa *et al.* data extend two magnitudes fainter for stars further than $40''$ from the cluster center. Qualitatively, Figures 5a-b show that our photometry is in reasonable agreement with previous efforts. Our zero-point error estimate of 0.04 mag seems reasonable in light of the comparison with previous photometry. We note that relative age determinations and blue straggler statistics are unaffected by absolute scale concerns, although the reddenings and distances determined will vary for different calibrations. We see no signs of non-linearity or color transformation problems that could affect the results discussed in this paper.

4. COLOR-MAGNITUDE DIAGRAMS

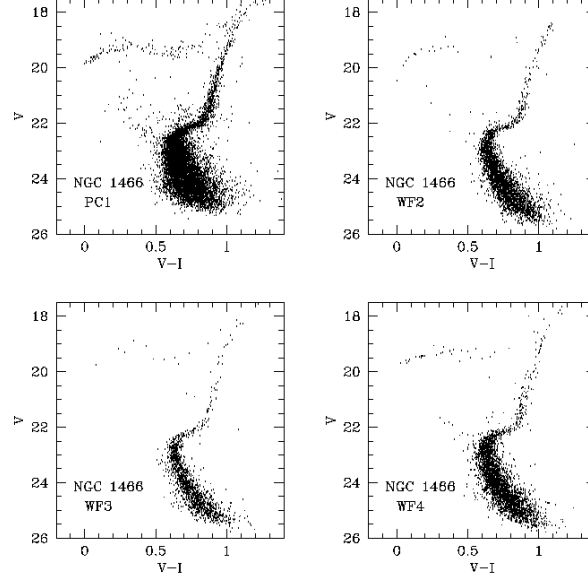


FIG. 6.—NGC 1466 color-magnitude diagrams for the individual chips of WFPC2. The cluster is centered on the PC1.

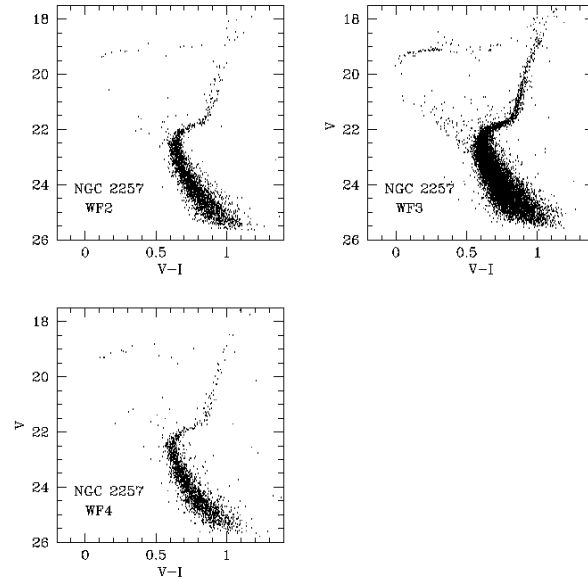


FIG. 7.—NGC 2257 color-magnitude diagrams for the individual chips of WFPC2. The cluster is centered on the WF3.

In Figures 6-8, we present the calibrated CMDs for the clusters. Zero-point differences cause slight offsets between the CMDs derived from the various chips within a given cluster. The largest shifts are ~ 0.025 mag in color, which can almost all be ascribed to the 0.015 mag random errors in the aperture corrections in V and I , with some error due to the Holtzman gain ratios and Whitmore & Heyer (1997) CTE corrections. In all cases we have well-defined cluster sequences from near the tip of the RGB down to ~ 3 mag fainter than the main-sequence turnoff (MSTO). We determined the fiducials for the stars on each chip using an algorithm described in Sandquist *et al.* (1996). The main-sequence fiducial was determined by binning the data in magnitude and finding the mode in color. The red-giant-branch (RGB) fiducial was found by using the mean

color of magnitude bins. The horizontal branch (HB) and sub-giant branch (SGB) could not be reliably fit by such methods, the HB because of the large color dispersion of the RR Lyr and the SGB because it was neither vertical or horizontal. In these two regions we found points by eye, but the spread in magnitude in these areas is small, and this procedure should not add large errors. For chips with a smaller number of stars, the bins used for finding the mode and mean were larger, and the fiducials are noisier. In Figures 9a-c, we plot the fiducials from each chip for each cluster. For NGC 2257 and Hodge 11, the clusters which have their centers on WF3, we used a sample with $r > 20''$ from the cluster center to determine the WF3 fiducial. For NGC 1466, we used stars with $r > 9''.2$ from the cluster center for the PC1 fiducial.

TABLE 4
CLUSTER FIDUCIAL POINTS

NGC 1466		NGC 2257		Hodge 11	
<i>V</i>	<i>V</i> − <i>I</i>	<i>V</i>	<i>V</i> − <i>I</i>	<i>V</i>	<i>V</i> − <i>I</i>
MS-SGB-RGB					
24.70	0.787	24.85	0.861	24.90	0.843
24.40	0.738	24.55	0.806	24.70	0.804
24.10	0.707	24.25	0.762	24.50	0.791
23.80	0.680	23.95	0.724	24.30	0.748
23.50	0.648	23.65	0.688	24.10	0.724
23.33	0.637	23.35	0.657	23.90	0.703
23.09	0.628	23.05	0.635	23.70	0.687
22.95	0.623	22.75	0.618	23.50	0.672
22.78	0.623	22.45	0.613	23.30	0.654
22.65	0.627	22.28	0.619	23.10	0.637
22.53	0.638	22.15	0.632	22.90	0.628
22.44	0.648	22.08	0.644	22.70	0.630
22.32	0.671	21.98	0.668	22.50	0.638
22.19	0.720	21.86	0.726	22.34	0.659
22.11	0.775	21.78	0.753	22.23	0.678
21.98	0.820	21.68	0.807	22.12	0.714
21.85	0.844	21.53	0.836	21.98	0.781
21.58	0.866	21.39	0.842	21.79	0.833
21.06	0.893	20.90	0.871	21.59	0.851
20.55	0.922	20.38	0.905	21.27	0.869
20.06	0.944	19.81	0.924	20.77	0.896
19.62	0.971	19.38	0.961	20.24	0.922
19.12	1.014	18.87	0.999	19.72	0.948
18.45	1.064	18.36	1.033	19.25	0.980
HB		HB		18.68	1.020
19.81	0.027	19.56	0.021	HB	
19.61	0.070	19.32	0.060	19.18	0.179
19.47	0.127	19.21	0.116	19.47	0.093
19.37	0.184	19.13	0.199	19.79	0.038
19.27	0.661	19.10	0.281	20.25	−0.010
19.20	0.771	18.95	0.723	20.76	−0.050
				20.80	−0.054

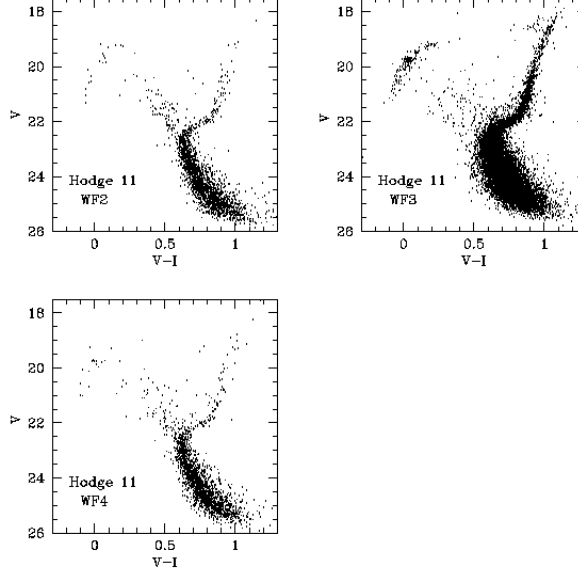


FIG. 8.— Hodge 11 color-magnitude diagrams for the individual chips of WFPC2. The cluster is centered on the WF3.

In our plot for NGC 2257, we include the fiducial determined from the inner $20''$ on WF3. It is offset by a constant color from the fiducial determined from the stars with $r > 20''$. We believe this is a manifestation of our less-than-perfect PSFs, which do not fully account for the changes in the PSF over the face of the chip. However, examination of Figures 9a-c shows that this is not a major concern, since the fiducials from each chip and each region look very similar.

For our final fiducials, we adopt the fiducial of the chip containing the cluster center (Table 4). We also calculated the shifts needed to compensate for chip-to-chip zero-point offsets by matching the SGBs and RGBs of the individual chip fiducials. These shifts were applied to the data to create a master CMD of all stars on all chips to use when finding blue stragglers.

5. RELATIVE AGES

5.1. Metallicities

In order to inter-compare the CMDs of the LMC clusters and to compare them with those for the GGCs, we need to know their metallicities. We will refer all measurements to the Zinn & West (1984; ZW84) scale. The accuracy of this scale has been questioned by Carretta & Gratton (1997). They determined [Fe/H] for individual stars in 24 GGCs using a homogeneous analysis of equivalent widths of Fe lines from high-resolution spectra. Their correlation with the ZW84 metallicities is significantly non-linear, especially for intermediate

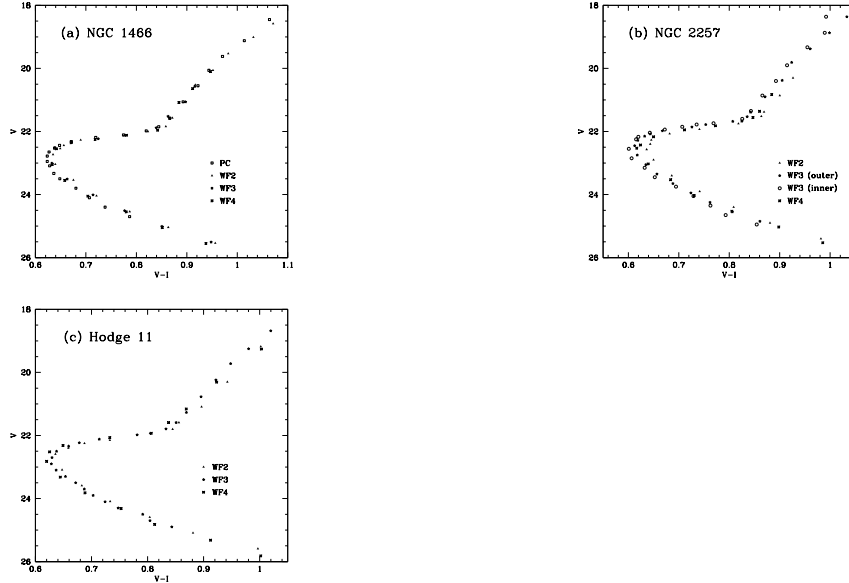


FIG. 9.— The fiducials determined separately from the data for each chip. (a) NGC 1466 (b) NGC 2257 (c) Hodge 11.

metallicities around -1.5 . Rutledge *et al.* (1997) compared metallicities based on W' , the reduced equivalent width of Ca II triplet lines, with ZW84 and Carretta & Gratton. This estimate of the metallicity also was related non-linearly to the ZW84 [Fe/H]'s, but linearly to the high-resolution results. This result is somewhat ambiguous because of the dependence of W' on $\log g$ and [Ca/Fe], but shows again that the relative, in addition to the absolute, scale of GGC metallicities has not been settled. However, we are interested in a small enough range that the ZW84 scale can be considered linear. Also, for relative age studies, sensitivity to [Fe/H] uncertainties decreases with decreasing Z and our results are not sensitive to [Fe/H] errors < 0.3 dex.

There are only a few studies of the abundances for the old LMC clusters. Cowley & Hartwick (1982) used low-resolution spectra to measure the G-band strength, Ca II break and the average strength of groups of weak Fe lines. They calibrated indices against several GGCs and used the Zinn (1980a) scale, which is almost identical to the ZW84 scale. Olszewski *et al.* (1991) measured the strength of the Ca IR Triplet lines for a large number of LMC clusters, including NGC 1466 and Hodge 11. They derive [Fe/H] via comparison with the Ca strength in stars in the GGCs NGC 288, NGC 1851, M 79 and NGC 7099 whose [Fe/H] were from ZW84.

For three stars in NGC 1466, Cowley & Hartwick found [Fe/H] $=-2.0 \pm 0.2$. Olszewski *et al.* (1991) derived abundances for two stars, LE4 and LE3, in NGC 1466 and found that LE4 had a substantially lower [Fe/H] (-2.48) than LE3 (-1.85). Walker (1992b) argued that since the apparent magnitude of LE4 placed it significantly above the cluster sequences, it probably had a close, bluer companion which weakened the Ca II equivalent widths. Checking our HST images, we find LE3 is reasonably well isolated, while LE4 is indeed blended with at least three other objects that are closer than $0''.5$. Walker also estimated [Fe/H] via several methods involving the properties of NGC 1466 RR-Lyrae stars and the de-reddened colors of various [Fe/H]-sensitive points in the cluster CMD. He found a consistent value of -1.82 ± 0.04 from all of his methods if $E(B-V)$ in the direction of NGC 1466 is ~ 0.08 mag.

Cowley & Hartwick measured three stars in Hodge 11 and derived a mean value of [Fe/H] $=-2.1 \pm 0.2$, consistent with Olszewski *et al.*'s average from two stars of -2.06 ± 0.2 . In this case, both stars had no companions within $0''.5$ on our HST frames. Based on the de-reddened color of the giant branch in $V-I$, Walker (1993), using the calibration of Da Costa & Armandroff (1990), derives [Fe/H] $=-2.0 \pm 0.2$ for $E(V-I)=0.1$.

For NGC 2257, Cowley & Hartwick measured a mean [Fe/H] $=-1.8 \pm 0.3$ from five stars. Testa *et al.* measured the metallicity indicator $(B-V)_{0,g}$ (Sandage & Smith 1966) from their CMD which leads to a value of -1.86 on the ZW84 scale. Walker (1989) used the period- A_B diagram of the RR Lyraes to estimate the metallicity as -1.8 ± 0.1 . The agreement between studies for each cluster is excellent.

We will adopt [Fe/H] $=-2.05$ for Hodge 11 and -1.85 for NGC 1466 and NGC 2257. These measurements are on the ZW84 scale, but in this [Fe/H] regime there is little disagreement between ZW84 and any of the more recent scales. The GGCs that we use for comparison are M 92 (-2.25) and M 3 (-1.66) (ZW84).

It is of potential concern that the LMC clusters could have different abundance ratios, such as [O/Fe], [C/Fe] and [α /Fe], than their Galactic counterparts. However, Cowley & Hartwick noted no difference in the metallicities derived by comparing

the strength of weak Fe lines to those of Galactic clusters and the metallicities found by looking at the Ca II break and the G-band, which are dominated by the abundance of the α elements. In the absence of any evidence to the contrary, we will assume the same trends in abundance ratios as are in GGCs.

5.2. Ages: CMD comparisons

Figures 10-12 show the fiducials for the LMC clusters compared to V , $V-I$ fiducials for M 92 and M 3 (Johnson & Bolte 1998).

We accounted for the differences in distance and small differences in abundance by registering the HB magnitudes at the blue edge of the RR Lyr gap so that $\Delta V_{HB} = -0.20\Delta[Fe/H]$. We accounted for the differences in reddening by making the relative colors of the RGB agree with Bergbusch & Vandenberg (1992) theoretical isochrones of the correct metallicity. In Figure 10a, the NGC 1466 fiducial line fits between M 92 and M 3 from the RGB (of course this is guaranteed by our procedure for correcting for $E(V-I)$ on the upper RGB) down through the MS as expected for a cluster with a metallicity intermediate between M 92 and M 3 and the same age as these two clusters. In Figure 10b, we show how well we can determine an age difference from such plots. We have taken Bergbusch & Vandenberg (1992) (BV92) isochrones for [Fe/H] $=-2.26$, -1.78 and -1.66 . On this plot, we represent M 92 and M 3 by 12 Gyr isochrones of [Fe/H] $=-2.26$ and -1.66 . Then we plot [Fe/H] $=-1.78$ isochrones for 13, 12, 11, 10 and 9 Gyrs. The differences in the turnoff region are striking and show that NGC 1466 has the same age as M 3 and M 92 to ≤ 1.5 Gyr. For NGC 2257 and Hodge 11, Figures 11-12 show the comparisons, and we reach similar conclusions.

5.3. Ages: Color-Difference Method

We can quantify the age differences between the GGC and the LMC clusters and among the LMC clusters themselves by measuring the color difference between the MSTO and the base of the RGB (VandenBerg, Bolte, & Stetson 1990 (VBS); Sarajedini & Demarque 1990). In practice, we do this by shifting the cluster fiducials horizontally until the colors of the MSTO match and vertically until a magnitude reference point matches. Since the MSTO does not have a well-defined magnitude, VBS suggested using the point on the MS that is 0.05 redder than the MSTO color ($V_{+0.05}$). All other things held constant, an older cluster will have a shorter SGB and, after MSTO registration, its RGB will lie to the blue of that for a younger cluster. Unfortunately, the length of the SGB also changes with metallicity. While this is a relatively small effect in $B-V$ (VBS), it is larger when $V-I$ colors are used. In $V-I$, the [α /H] is the crucial abundance to know (VandenBerg, private communication) and in all cases we have a good relative metallicities from Ca lines. To determine the magnitude of the metallicity effect requires the use of theoretical isochrones, and in particular, theoretical colors. Since colors are among the most uncertain quantities predicted by theory, we will use two separate sets of isochrones to evaluate our results and their dependence on the choice of isochrones.

Our LMC fiducials are in many ways an ideal dataset to use with this method. They were all taken with the same instrument and have the same data quality. They have low metallicities within 0.2 dex of each other, so the effects on the colors are minimized. We measured the MSTO color by fitting a parabola to the individual points in that region. We then interpolated between our fiducial points on the MS to determine $V_{0.05}$. In

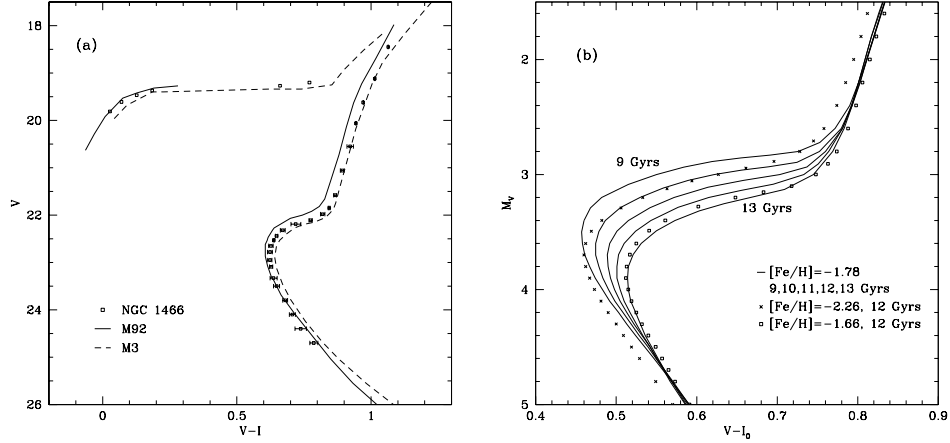


FIG. 10.— (a) NGC 1466's fiducial compared with M 92 and M 3. We have two estimates of the error in the NGC 1466 points. First, we determined the average deviation of the PC fiducial from the WF fiducials in Figure 9a. Second, we estimate the random error in the color of each bin to be 0.005 magnitudes. We adopted the larger number as our error. The V errors in the HB magnitude are smaller than the boxes used. However, the M 92 and M 3 HBs have larger, but unknown, errors because of the relatively few stars that define them (see Johnson & Bolte 1998 for more discussion). (In particular, the blue end of M3's HB is defined by one star.) (b) Bergbusch & Vandenberg (1992) isochrones compared in a similar manner. Isochrones of 12 Gyrs are plotted for $[\text{Fe}/\text{H}] = -2.26, -1.78$ and -1.66 . To illustrate the effect of age, $[\text{Fe}/\text{H}] = 1.78$ isochrones are also plotted for 9, 10, 11, and 13 Gyrs. ($[\text{Fe}/\text{H}] = 1.78$ is more metal-rich than the values (c.f. Table 1) for our clusters, so the correct isochrones would be bluer and brighter.)

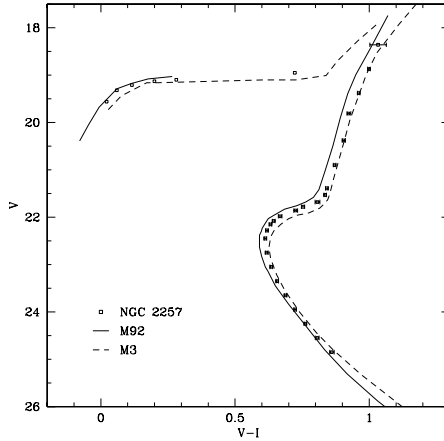


FIG. 11.— NGC 2257's fiducial compared with M 92 and M 3. See the caption for Figure 10 for a discussion of the errors.

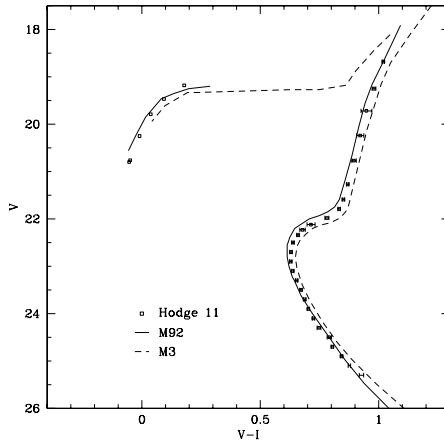


FIG. 12.— Hodge 11's fiducial compared with M 92 and M 3. See the caption for Figure 10 for a discussion of the errors.

Figure 13 we have registered the LMC cluster fiducials using

these two points. The sequences for NGC 1466 and NGC 2257

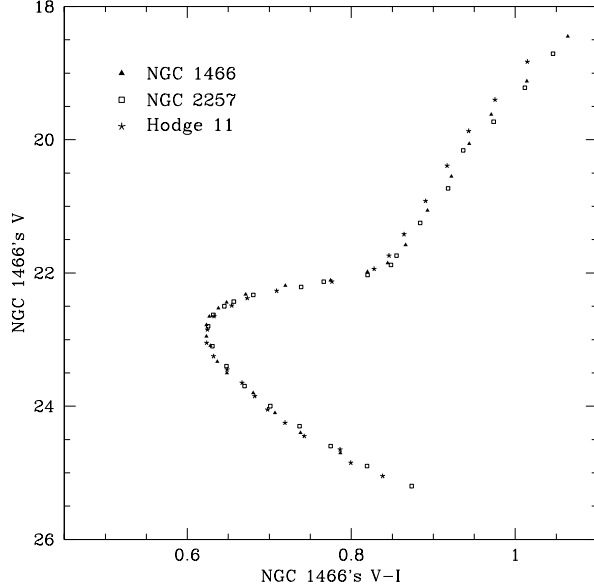


FIG. 13.—NGC 1466, NGC 2257 and Hodge 11 fiducials compared using the color-difference method. The remarkable agreement in the position of their RGBs, especially for NGC 1466 and NGC 2257, argues against a large age difference between the clusters.

are indistinguishable. Hodge 11's RGB lies to the blue of the other two. With the color-difference method in $V-I$, the more metal-poor Hodge 11 should be redder than NGC 1466 and NGC 2257, so this indicates that Hodge 11 is somewhat older than the other two. As shown below, the derived age difference is not large.

Next, we quantified the age difference between the LMC clusters and the GGCs based on any shifts of the positions of the registered RGBs. We first fit the GGCs RGBs from the base to the magnitude of the HB with a straight line. Next, we calculated the weighted average of the color offset between these lines and the individual RGB stars below the HB of each of our LMC clusters. In Figure 14, we show an example of the method where we have registered M 92 and NGC 2257 using the two fiducial points. Based on VBS, the *mean* offset for a cluster gives the age difference (compared to M 92) and the standard error of the mean offset gives an estimate of our δ age precision. The mean offsets for each cluster are recorded in Tables 5a-b as $\delta(V-I)$.

While the standard error of the mean represents the error in our measured shifts caused by scatter on the RGBs, it does not take into account errors in our choice of $V-I_{MSTO}$ and $V_{+0.05}$. The error in $V_{+0.05}$ caused by scatter on the MS has only a small effect on the color shift of the RGB since the RGB is almost vertical. A shift of 0.05 mag in $V_{+0.05}$ results in a color shift of 0.0025 mag. The more significant error is in $V-I_{MSTO}$. This color could change by an amount of order $V-I \sim 0.003$ mag if we made plausible alterations in the fitting range and the acceptable color error for our parabolic fit. We conservatively estimate our observational error in $V-I_{MSTO}$ as 0.005 mag. Unfortunately, an error in the color also results in an error in our choice of $V_{+0.05}$. These two errors work in the same direction. For example, if our MSTO color is too red, our $V_{+0.05}$ will be too faint. We will then shift our fiducial too far to the blue to get our red MSTO color to match and too bright (and hence too blue) to get our $V_{+0.05}$ to match. Taking into consideration the slopes of the MS and the RGB, we find that our 0.005 mag er-

ror in color results in an additional 0.0035 mag shift in the RGB color due to the correlation of these errors. Our total random error is therefore 0.009 mag. Finally, we note that since we calculate the difference for our three LMC clusters relative to one GGC at a time, the errors in the GGC points will result in a systematic shift. Comparing the results obtained for M 92 in Table 5a with those for M 3 in Table 5b will provide an estimate of the size of that effect.

To convert our measured $\delta(V-I)$ and errors into age differences and uncertainties, we used two sets of isochrones: Bergbusch & Vandenberg (1992) (BV92) and the new Yale Isochrones (Chaboyer *et al.* 1995) (C95). We determined the predicted shifts in RGB color as functions of metallicity and age after registering the isochrones in the same manner as our data. For $-1.66 > [\text{Fe}/\text{H}] > -2.26$, we found that the color shift predicted by BV92 depends on the metallicities by the following relation:

$$\delta(V-I) = -0.069(\Delta[\text{Fe}/\text{H}]). \quad (1)$$

Next, comparing sets of isochrones with the same metallicity, but with ages ranging from 9 to 13 Gyrs, we found that the RGB shift is related to the age difference (in Gyr) by

$$\delta(V-I) = -0.021(\Delta\text{Age}). \quad (2)$$

We first removed the known shift due to metallicity differences from our results in Tables 5a-b. The remaining shift is due to age differences. Using our age- $\delta(V-I)$ relation above, we calculated the age differences relative to the GGCs and included those values in Tables 5a-b. Our age- $\delta(V-I)$ relation is valid only for ages between 9 and 13 Gyrs. Our use of younger isochrones to calibrate the RGB shifts is not crucial for our discussion of relative ages, but we note that the choice of an older age range would increase the implied age difference for a given $\delta(V-I)$. However, the errors would also increase, and we would be left with the same conclusion.

We performed the same procedure using the C95 isochrones with two exceptions. First, the C95 isochrones are not α -

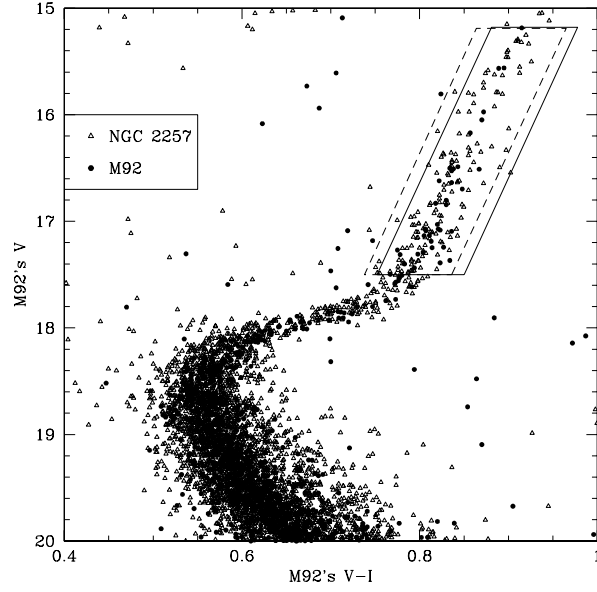


FIG. 14.—The color-difference method applied to NGC 2257 and M 92. We plotted the individual stars for each cluster. The solid trapezoid shows the M 92 stars used to calculate the straight line fit to the RGB. The dashed trapezoid encloses the NGC 2257 stars used to calculate the RGB shift relative to the M 92 line.

TABLE 5A
 $\delta(V-I)$ QUANTITIES

Cluster	$(V-I)_{TO}$	$V_{+0.05}$	$\delta(V-I)$	Δ Age (Gyrs) (BV92)	Δ Age (Gyrs) (C95)
M 92	0.553 ± 0.008	19.45 ± 0.05	0.000 ± 0.014	0.0 ± 0.7	0.0 ± 0.7
NGC 1466	0.623 ± 0.005	23.73 ± 0.05	-0.012 ± 0.009	-0.8 ± 0.4	-1.0 ± 0.5
NGC 2257	0.610 ± 0.005	23.38 ± 0.05	-0.008 ± 0.009	-1.0 ± 0.4	-1.2 ± 0.5
Hodge 11	0.628 ± 0.005	23.58 ± 0.05	-0.021 ± 0.009	$+0.3 \pm 0.4$	$+0.3 \pm 0.5$

TABLE 5B
 $\delta(V-I)$ QUANTITIES

Cluster	$(V-I)_{TO}$	$V_{+0.05}$	$\delta(V-I)$	Δ Age (Gyrs) (BV92)	Δ Age (Gyrs) (C95)
M3	0.595 ± 0.005	19.92 ± 0.05	0.000 ± 0.009	0.00 ± 0.4	0.00 ± 0.5
NGC 1466	0.623 ± 0.005	23.73 ± 0.05	0.008 ± 0.009	$+0.24 \pm 0.4$	$+0.36 \pm 0.5$
NGC 2257	0.610 ± 0.005	23.38 ± 0.05	0.011 ± 0.009	$+0.10 \pm 0.4$	$+0.21 \pm 0.5$
Hodge 11	0.628 ± 0.005	23.58 ± 0.05	-0.002 ± 0.009	$+1.28 \pm 0.4$	$+1.56 \pm 0.5$

enhanced, so we followed their recommendation and determined the appropriate solar-scaled isochrones by using the formulation of Salaris, Chieffi, & Straniero (1993) and choosing the relative α abundances to be $4\times$ solar. Second, we found a noticeable trend in the steepness of the slope of the age- $\delta V-I$ relation depending on the metallicity of the isochrones. However, this affected our ages only at the level of 0.05 Gyrs, so we adopted the slope determined from the $[\text{Fe}/\text{H}] = -1.66$ isochrones. Our equations for $\delta(V-I)$ versus metallicity and age are

$$\delta(V-I) = -0.080(\Delta[\text{Fe}/\text{H}]), \quad \text{and} \quad (3)$$

$$\delta(V-I) = -0.020(\text{Age}) \quad (4)$$

The C95 isochrones have a steeper dependence on metallicity, but the overall agreement between BV92 and C95 is quite good. The calibration of the color-difference method will need to be updated again as newer isochrones become available, but there is no evidence that the theoretical calibration will be an overwhelming source of error. Based on the $\delta(V-I)$ method, we conclude that the LMC clusters are the same age as the GGCs to within 1.5 Gyrs.

5.4. Ages: V_{BTO}

The relative ages of GCs can also be calculated by using the difference in V magnitude between the HB and the MSTO (the ΔV method) (Sandage 1982). Because luminosities can be predicted more reliably than temperatures, this method has been often put forward as the most robust of the relative age estimators. However, it is relatively more uncertain for clusters with very blue HB morphologies such as Hodge 11 for at least two reasons. First, it is difficult to assign an apparent brightness to the HB and to correct for HB-star evolution in blue-HB clusters. Second, as pointed out recently by Sweigart (1997) and Langer, Bolte & Sandquist (1999), there is reason to suspect that some blue HB stars have had helium mixed into their envelopes resulting in higher HB luminosity and, for clusters containing He-mixed stars, an artificially inflated ΔV value. In addition, our M 3 and M 92 data do not have many HB stars, which limits the precision of our HB magnitudes. Finally, determining the magnitude of the MSTO is uncertain, since the color-magnitude diagram is vertical at that point.

Chaboyer *et al.* (1996a) proposed a modification that moved the lower reference point to the subgiant branch, 0.05 mag redder than the MSTO color (V_{BTO}). This reduces the errors, since the CMD cluster sequence is sloped at that point and a fiducial point can be determined with more confidence. To find V_{BTO} , we used the mean magnitude of the stars in a box on the subgiant branch centered on our fiducial at $(V-I)_{MSTO} + 0.05$. The box was 0.04 mag wide in color and 0.15 mag wide in V . The standard error of the mean for those points within the box provides one estimate of the error, but probably underestimates it because there is additional confusion at the blue end of the SGB due to the scatter of stars from the MS to the red. This makes the SGB wider in magnitude and makes V_{BTO} dependent on our exact box size in vertical direction. Our total errors are therefore closer to ~ 0.03 mag. For the HB magnitude of NGC 1466 and NGC 2257, we found the average and the standard error of the mean for our HB stars at the blue end of the RRLyr gap. This is the method by which we found the HB magnitude for our GGC data, and avoids the problem of determining $\langle M_V(\text{RR}) \rangle$ with our limited time resolution. We used the HB of NGC 2257

as a template to extend Hodge 11's extremely blue horizontal branch to the red. We ignored the two reddest points of the Hodge 11 HB as likely being either evolved stars or field interlopers. The Hodge 11 HB magnitude derived in this manner is very uncertain. Table 6 summarizes our values for V_{HB} and V_{BTO} .

To convert V_{BTO} to $M_V(BTO)$, we adopt the relationship from Gratton *et al.*'s (1997) analysis of the Hipparcos data,

$$M_V(HB) = 0.17([\text{Fe}/\text{H}] + 1.5) + 0.39. \quad (5)$$

In choosing this relationship for the magnitude of the HB, we are implicitly choosing absolute ages for the globular clusters of about 12 Gyrs. As we discuss in §5.3, this affects the precision of our results, but it does not affect our conclusions.

Chaboyer *et al.* (1996a) provide the conversion between $M_{V(BTO)}$ and age for V, I data for five metallicities. The relevant equations for our discussion are

$$t_9 = 70.7 - 48.5M_{V(BTO)} + 9.3M_{V(BTO)}^2 \quad [\text{Fe}/\text{H}] = -2.5 \quad (6)$$

$$t_9 = 71.4 - 47.5M_{V(BTO)} + 8.8M_{V(BTO)}^2 \quad [\text{Fe}/\text{H}] = -2.0 \quad (7)$$

$$t_9 = 86.3 - 53.5M_{V(BTO)} + 7.3M_{V(BTO)}^2 \quad [\text{Fe}/\text{H}] = -1.5 \quad (8)$$

For all these clusters, we used the equation valid for $[\text{Fe}/\text{H}] = -2.0$ to derive ages (Table 6). This is too metal-poor for NGC 1466, NGC 2257 and M 3 and too metal-rich for M 92, and metallicity does affect the magnitude of the MSTO. To estimate the size of this effect, we used M 3's $M_{V(BTO)}$ to find its age using equations (7) and (8), which bracket M 3's $[\text{Fe}/\text{H}]$. We then assumed a linear relationship between $\Delta[\text{Fe}/\text{H}]$ and ΔAge and found that we should make M 3's age younger by ~ 0.6 Gyrs to account for the 0.20 dex difference in metallicity. This is still consistent with being co-eval with NGC 1466 and NGC 2257. A similar calculation using equations (6) and (7) suggests that M 92's age should be 0.8 Gyrs older. The errors shown for ΔAge in Table 6 include only the observational errors and not possible errors from incorrect metallicities or distances. Hodge 11 appears to be 2 Gyrs older by this method, but there is a large additional component in the error due to the uncertainty in setting the HB level. These calculations confirm our result in the previous sections.

Each method of calculating relative ages suffers from both systematic and random uncertainties. However, by using a combination of these methods, we can hope to determine the allowable age differences. Despite potential problems with finding HB magnitudes, relying on theoretical isochrones for calibration of age differences in color and magnitude, calculating fiducials for clusters with different crowding conditions and using the *HST* calibrations, we consistently find no large age differences between M 92 and M 3 on one hand and NGC 1466, NGC 2257 and Hodge 11 on the other. Unless one of these methods is found to suffer from a serious flaw, a reasonable statement is that the GGC and these LMC clusters have the same age ± 1.5 Gyr. However, we find that Hodge 11 consistently looks a little older. This may be due to an actual age difference, but the ΔV measurement in particular could be due to the mixing of helium into the envelope, as discussed above.

TABLE 6
 V_{BTO} QUANTITIES

Cluster	$(V-I)_{TO}$	V_{BTO}	V_{HB}	q1head $M_{V(BTO)}$	Δ Age (Gyrs)
M3	0.595	18.65 ± 0.05	15.75 ± 0.05	3.26 ± 0.07	0.0 ± 0.8
M92	0.553	18.14 ± 0.05	15.18 ± 0.08	3.22 ± 0.09	-0.4 ± 0.8
NGC 1466	0.623	22.33 ± 0.03	19.32 ± 0.01	3.34 ± 0.03	0.8 ± 0.4
NGC 2257	0.610	22.04 ± 0.03	19.10 ± 0.01	3.27 ± 0.03	0.1 ± 0.4
Hodge 11	0.628	22.25 ± 0.03	19.11 ± 0.1	3.44 ± 0.10	2.0 ± 1.5

The extremely blue HB of Hodge 11, bluer than the more metal-poor M 92, would agree with either an age difference or helium-mixing.

5.5. Distances

The distance to the LMC is an important and controversial quantity (see *e.g.*, Westerlund 1997 for a review). The LMC provides a testing ground for consistency between the Cepheid and RR Lyrae distance scales. Recent estimates for the LMC distance modulus have ranged from $(m-M)_0 = 18.05$, based on observations of “red clump” stars (Stanek, Zaritsky & Harris, 1998), to $(m-M)_0 = 18.7$, based on Cepheid properties (Feast & Catchpole 1997). Fernley *et al.* (1998) used Hipparcos proper motions for Galactic RR Lyrae stars and statistical parallax to derive $(m-M)_0 = 18.26$. The most recent estimate based on the illumination of the SN1987a ring is $(m-M)_0 < 18.44$ (Gould & Uza 1998). Generally, the RR-Lyrae-based distance to the LMC has been smaller than that set by Cepheid observations (see *e.g.*, Walker 1992a). Adding to the confusion is the possibility that RR-Lyrae stars in the LMC may have systematically different luminosities than Galactic RR Lyraes (Walker 1992a; van den Bergh 1995).

We can use our data to examine these issues by determining the relative distance moduli between the LMC clusters and M 92 via (1) matching HB levels and (2) matching the unevolved main-sequence (MS) positions. Our data extend far enough down the MS that we can use method (2). Because of the steep slope of the main sequence, the color offset due to reddening and systematic errors in $V-I$ must be removed before the MSs can be matched vertically. We do this by shifting the RGBs to their expected relative positions and then adjusting the distance moduli to match the MSs. This is an iterative process, and not as precise as knowing the reddening separately. We find that our range of acceptable fits leads to errors in the distance moduli of ~ 0.05 mag. As can be seen in Figures 10 through 12, *we would have derived identical relative distances if we had matched the HBs of the clusters*. This latter observation strongly suggests that there is no large difference (~ 0.3 mag) in the luminosity of HB stars between the LMC clusters and M 92. We then corrected these distance moduli for the differential extinction between M 92 and these clusters. We adopted the reddening of Walker (1992a) for our LMC clusters and $E(B-V) = 0.02$ mag for M 92 (Harris 1996). These true distance moduli between M 92 and the LMC clusters are listed in Table 7 as $\mu_{M92,GC}$.

As discussed earlier, our *HST* zeropoints have errors ~ 0.04 mag, due to uncertain aperture and CTE corrections and the accuracy of the Holtzman *et al.* calibration. To provide a comparison with a ground-based reference, in Table 7 we in-

clude our HB magnitudes and Walker’s $\langle M_V(RR) \rangle$ corrected by 0.04 mag for the offset between RR Lyrae magnitudes and HB level (Gratton *et al.* 1997). Added to this photometric uncertainty are our uncertainties in the MS-fitting and in the differential reddening. If we take 0.03 mag as an estimate of the uncertainty in the differential reddening, then our error per cluster is ~ 0.07 mag.

We prefer the Pont *et al.* (1998) M 92 distance as it is based on a larger, better-selected sample of subdwarfs. The distance moduli for M92 and our clusters are listed in Table 7 as $\mu_{\odot,GC}$. Using this, our LMC distance modulus from the average of our clusters’ distances is $m-M \sim 18.49$. To illustrate the systematic uncertainty still remaining because of the dispute over the local distance scale, we include in Table 7 the distance moduli we derive using the Gratton *et al.* (1997) distance to M 92. As for our measuring error, the MS-fitting error and at least half of the zeropoint error are random. The systematic errors, such as the errors in the gain ratios of the chips are mitigated because the center of the cluster is not always on the same chip. Our clusters are also not at the center of the LMC. We have attempted to correct for this by assuming that the clusters lie in the HI disk (inclination 29° , PA of nodes -9°) as argued by Schommer *et al.* (1992). Our derived distances for the LMC center are included in Table 7 ($\mu_{\odot,LMC}$). This changes our LMC distance modulus only slightly to 18.52 mag. In fact, if the clusters lie in a disk, then our distance measurement is relatively immune to changes in the assumed inclination and PA of the nodes because NGC 1466 and NGC 2257 have about the same projected distance from the LMC center but are on opposite sides of the LMC center, while Hodge 11 is fairly close to the LMC center. For our final error budget, we include the 0.07 mag per cluster divided by $\sqrt{3}$ plus 0.03 mag error in our averaged number due to uncertain geometrical corrections. Also, Pont *et al.* quote 0.08 mag as their error in the distance modulus to M92. Our final $(m-M)_0$ is 18.46 ± 0.09 mag.

5.6. Blue Stragglers

All three of our clusters have a prominent blue-straggler star (BSS) sequence. To see how the frequency of BSS in these clusters compares with that in GGCs, we used the specific frequency, F_{BSS} , defined by Bolte, Hesser & Stetson (1993) to be the ratio of the number of BSS to the number of stars with $V < V_{HB} + 2$. Before we can count stars in either category, we need to make two corrections. First, even the 260s frames were long enough to saturate the brightest RGB and AGB stars in the clusters and therefore they do not appear on our CMDs. However, by looking at our images and star lists, it is easy to find the number of bright stars (~ 15) that are not on the list (Table

TABLE 7
DISTANCE MODULI

Cluster	A_V	$\mu_{M92,GC}$	$\mu_{\odot,GC}$ Pont	$\mu_{\odot,LMC}$ Pont	$\mu_{\odot,GC}$ Gratton	V_{HB}	“ V_{HB} ” Walker
M92	0.06	14.61	14.74	15.18
NGC 1466	0.29	3.97	18.58	18.42	18.71	19.32	19.29
NGC 2257	0.13	3.78	18.39	18.55	18.52	19.10	18.99
Hodge 11	0.25	3.89	18.50	18.59	18.63	19.11

TABLE 8
STELLAR POPULATION STATISTICS

Cluster	# “BS” “cluster”	# “BS” “field”	# RGB/HB/AGB ($V < V_{HB} + 2$) “cluster”	# Saturated colheadStars	# RGB/HB/AGB ($V < V_{HB} + 2$) “field”	Ratio ClusterArea FieldArea
NGC 1466	73	0	721	17	26	1.41
NGC 2257	67	5	422	16	44	1.64

8).

The larger correction is due to field-star contamination in the BSS region. The analysis of Hodge 11 is severely hampered by this, and we will not determine F_{BSS} for this cluster. For the “BSS region” in the CMD, we adopted a box with magnitude boundaries at $V_{+0.05} - 1.0$ and $V_{+0.05} - 3.0$ and color boundaries at $V-I_{MSTO} - 0.1$ and $V-I_{MSTO} - 0.6$ (see Figures 15-16). These boundaries are somewhat arbitrary and are on the conservative side (*i.e.*, they minimize contamination from the MSTO, but also may miss some BSS). For NGC 1466 and NGC 2257, our total sample consists of the stars from all the chips, with the shifts discussed in §4 applied (this step makes very little difference). To estimate the field contamination, we divided our sample at $r = 80''$. The outer stars are not a true field population, but will provide an upper limit on the number of interlopers we might expect.

In Figures 15 and 16, we show the upper CMD of both the “field” and the “cluster” populations with the BSS region marked. The number of stars in each region is included in Table 8. (We note that all of the saturated stars belong to the “cluster” sample.) NGC 2257 and NGC 1466 have F_{BSS} of 0.14 and 0.10, respectively. For these numbers, we have only subtracted our “field” contamination from the blue straggler region. We have not considered contamination from field stars in the RGB+AGB+HB region. Examination of the CMDs of stars further away from the cluster in Walker (1992b) and Testa *et al.* (1995) show that the number of field stars is about equal in both regions. Since we have so many bright RGB+AGB+HB stars compared to blue stragglers, possible contamination in this region will not affect our results significantly. In Table 9 we list the F_{BSS} of some GGCs. In this group we include new numbers for Eridanus, Pal 3, Pal 4, and NGC 2419 based on the HST observations of Stetson *et al.* (1999) and Harris *et al.* (1997) and using our definition of BSSs.

6. DISCUSSION

6.1. Blue Stragglers: F_{BSS}

The globular clusters listed in Table 9 have remarkably similar F_{BSS} . There are, of course, systematic differences among the studies in their completeness, in crowding effects and in the blue straggler definition. However, while there may be factors of up to two obscured by such problems, factors of ten are very unlikely, based on comparing studies of the same cluster with different completeness limits and crowding conditions. We have chosen mainly other HST studies to include in Table 9, which also makes the sample more homogeneous. The relatively narrow range in F_{BSS} , compared to the 10^4 range in cluster central densities, was noted by Sosin & King (1995). They argued that as the cluster density changes, different mechanisms (*e.g.*, stellar collisions, tidal capture, merging of primordial binaries) become important for the formation of blue stragglers. Although the efficiency of the various mechanisms varies from cluster to cluster, the total production rate stays approximately constant. Our new data strengthen this point. Eridanus has a F_{BSS} at the high end of the range and close to that of M 30. M 30 is a post-core-collapse cluster with a central mass density $\log(\rho_0) = 5.26$. Eridanus, on the other hand, is a sparse cluster at large Galactic radius. Its $\log(\rho_0)$ is of order 0.5 (Webbink 1985). The blue straggler specific frequencies for NGC 1466 and NGC 2257 show that clusters belonging to other galaxies have the same constraints on the rate of blue straggler formation as those of the Galaxy.

6.2. Ages and Age Distribution

6.2.1. Previous Results

The principle result of this study is that these three LMC clusters are the same age as M 92 and M 3 to a precision of 1.5 Gyr. Michell *et al.* (1996) previously reported that Hodge 11 and M 92 have the same age to within 10 to 21%. Testa *et al.* (1995), based on a comparison of fiducial sequences and ΔV values, found that NGC 2257 was about 2 Gyrs younger

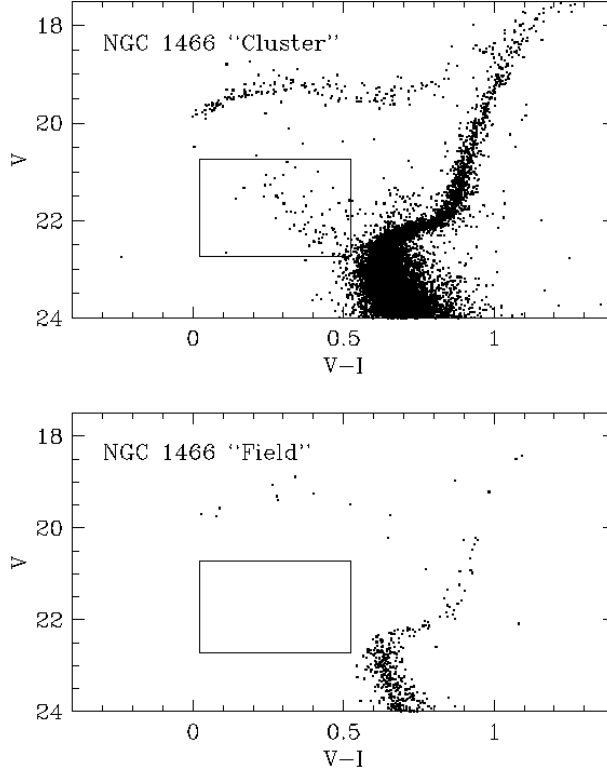


FIG. 15.— The upper part of the CMD of NGC 1466 with the blue straggler box marked. The upper panel shows the stars with $r < 80''$ and the bottom with $r > 80''$. There is very little field contamination evident in the “field” plot.

TABLE 9
BLUE STRAGGLER FREQUENCIES

Cluster	F_{BSS}	Survey Region	c	Source for F_{BSS}
Milky Way Globulars				
M 30	0.19 ± 0.04	$r \leq 10r_{core}$	2.40	Yanny <i>et al.</i> 1994
NGC 6624	0.13 ± 0.14	$r \leq 1.0r_{core}$	2.15	Sosin & King 1995
47 Tuc	0.07 ± 0.01	$r \leq 3.0r_{core}$	2.08	Guhathakurta <i>et al.</i> 1992
M 3	0.09 ± 0.02	$r \leq 0.7r_{core}$	1.89	Guhathakurta <i>et al.</i> 1994
M 13	$0.04 - 0.09$	$r \leq 1.7r_{core}$	1.44	Cohen <i>et al.</i> 1997
NGC 2419	0.06 ± 0.005	$r \leq 8.2r_{core}$	1.40	Harris <i>et al.</i> 1997
Eridanus	0.18 ± 0.05	$r \leq 8.4r_{core}$	1.14	Stetson <i>et al.</i> 1999
Pal 3	0.15 ± 0.05	$r \leq 4.2r_{core}$	0.96	Stetson <i>et al.</i> 1999
Pal 4	0.12 ± 0.04	$r \leq 4.9r_{core}$	0.78	Stetson <i>et al.</i> 1999
NGC 5053	0.14 ± 0.03	$r \leq 1.0r_{core}$	0.77	Nemec & Cohen 1989
LMC Globulars				
NGC 1466	0.10 ± 0.01	$r \leq 5.4r_{core}$	1.42	this paper
NGC 2257	0.14 ± 0.02	$r \leq 3.2r_{core}$	1.10	this paper

NOTE.—Structural parameters for GGCs from Trager *et al* (1993) and for LMC from Mateo (1987).

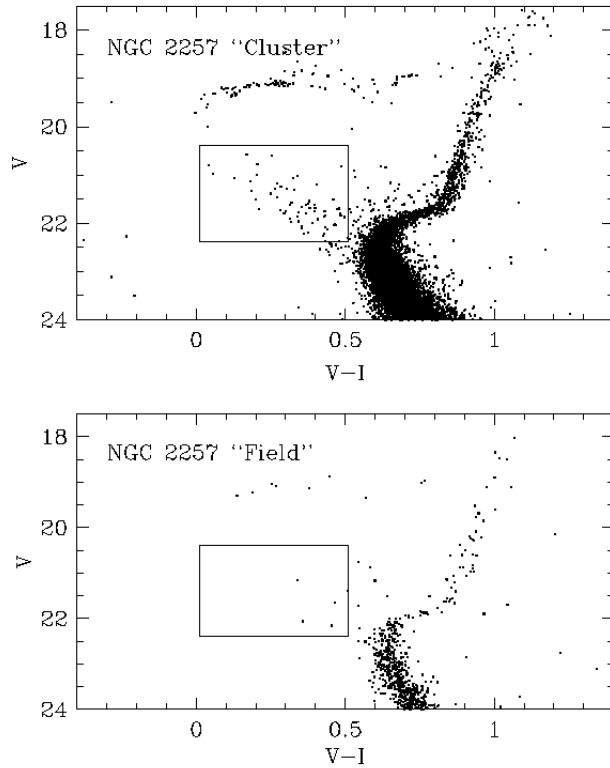


FIG. 16.— The upper part of the CMD of NGC 2257 with the blue straggler box marked. The upper panel shows the stars with $r < 80''$ and the bottom with $r > 80''$. While there are some stars in the blue straggler box in the outer sample, the overall diagram shows very little evidence for field contamination. Therefore our derived F_{BS5} is most likely a lower limit.

than NGC 5897 and M 3. In §5.4, we found that a modified ΔV method gives similar ages for M 3 and NGC 2257. Part of the discrepancy lies in the smaller ΔV value of 3.45 we find for M 3 (Johnson & Bolte 1998). We note that Stetson *et al.* (1998) found a ΔV of 3.46 for M3. Their sample included the Johnson & Bolte stars, but was about twice as large, including having more HB stars.

There are two other major studies of the ages of other old clusters in the LMC. Brocato *et al.* (1996) argued on the basis of ΔV measurements that NGC 1786, NGC 2210 and NGC 1841 have the same age as the mean age of the GGCs, although their precision was about ± 3 Gyrs. Olsen *et al.* (1998) (O98) found that the ages of four old LMC clusters were the same as M 5 or M 55. One cluster, NGC 1835, was 2 Gyrs older than M 3. Depending on the age difference between M 3 and M 5, this could mean than NGC 1835 was coeval with the other O98 clusters. Another significant result from their paper was the determination of the metallicities of their clusters from the morphology of the RGB. They found metallicities about 0.2 dex higher than those found by Olszewski *et al.* (1991).

Before we can put all the above results together, including ours, we need to consider possible age differences between the GGC samples used to compare with the LMC ones. Lee *et al.* (1994) argued on the basis of HB morphology that GGCs with $R_{GC} < 8$ kpc are on average 2 Gyrs older than those between 8 and 40 kpc. M 5 (6.4 kpc) and M 55 (4.2 kpc) fall into the inner group while M 3 (8.5 kpc) and M 92 (9.1 kpc) are members of the outer, possibly younger halo (although note that the orbit of M 5 carries it into the outer halo). Without resolving the issue of the chronology of GGC formation, we will discuss results for the GGCs listed above. Table 10 summarizes the recent relative ages for these four clusters obtained from the literature.

It is apparent that widely varying opinions exist on the age spread in the Galactic halo. Part of this is due to observational uncertainties. Our value for the HB magnitude of M 92 (15.18) is considerably fainter than the 14.96 used by Chaboyer *et al.* (1996b) and Gratton *et al.* (1997). If our value is correct, then the age gap between M 92 and the other clusters will be reduced. However, although uncertainties still exist, the outer halo clusters M 92 and M 3 are apparently not younger than the inner halo M 5 and M 55. We can directly compare our LMC fiducials to the inner-halo GGC M 55, which has a metallicity, $[Fe/H] = -1.85$ (ZW84), about the same as our LMC clusters. G. Mandushev kindly sent us the V, V-I photometry of Mandushev *et al.* (1996). We choose the NGC 2257 fiducial as representative of our LMC clusters. Figure 17 shows that the two cluster fiducials match very closely throughout the CMD. As is the case for the LMC-M 92 comparison, there is at most a small, < 1.5 Gyr, age difference between NGC 2257 and M 55.

6.2.2. Implications for the Formation of the Local Group

The LMC has been suggested as the prototype of a source for present-day GGC. One of the scenarios advocated by Searle & Zinn (1978) was that clusters formed in “fragments”, perhaps small gas-rich irregulars, that evolved and interacted over the span of several billion years. In the particular case of the LMC, Zinn (1980b, 1993) has suggested that satellites like the LMC contributed their GCs to the MW halo. Previous observations of the LMC clusters revealed that they are similar to the GGC in many respects (see Suntzeff *et al.* 1992). Suntzeff *et al.* pointed out that the GGC system could have been made by merging ~ 8 LMC-like objects. Van den Bergh (1996) found, on the other hand, that the metallicities of the old LMC clusters

in the Suntzeff *et al.* sample were, on average, lower than those for clusters in the MW’s outer halo. The increased metallicity estimates by O98 for five of the old LMC clusters would make this discrepancy smaller. Van den Bergh & Morbey (1984) and others also argued that since the ellipticity of the LMC clusters is greater than in the MW clusters, it was unlikely that the MW had captured LMC clusters. The LMC clusters have a larger average ellipticity regardless of the age range considered, although at the time, accurate ages were not available. Here we consider only those LMC clusters that have been confirmed as old and that have ellipticity measurements by Frenk & Fall (1982) and those MW clusters that are not heavily reddened ($E(B-V) < 0.32$) (Harris 1992). A two-sided K-S test can reject only at the 77% level the hypothesis that these two groups were drawn from the same distribution. Goodwin (1997) notes that cluster ellipticity can depend more strongly on the tidal field of the parent galaxy than it does on intrinsic cluster properties. For the specific case of the three LMC clusters considered here, each of them has a small eccentricity, consistent with the distribution seen in the GGCs.

Another similarity between the old clusters of the Galaxy and LMC is in the distribution of HB morphology with $[Fe/H]$. In the outer halo of the Galaxy, the HB morphology of GGCs is on average too red for the cluster metallicity (the “young halo” of Lee *et al.* 1994). Zinn (1993) showed that the best match to the outer halo GGC properties in terms of $[Fe/H]$ and HB morphology were the clusters of the LMC and SMC. (In fact, the SMC globular NGC 121 was the first “second parameter” globular cluster noticed (van den Bergh 1967)). He suggested that the majority of the inner halo clusters formed in the overall collapse of the Galaxy, but that the outer halo was mostly accreted from relatively large satellites.

The new *HST* results allow us to make a few comments about the scenario in which LMC-like galaxies are absorbed by the Galaxy and contribute their stars to the Galactic halo. On the basis of age, the old LMC clusters would be indistinguishable from existing GGCs, at least our comparison clusters in the intermediate halo. With the recent age estimates and, for the O98 clusters, revisions in $[Fe/H]$ estimates, it is also possible to improve on the $[Fe/H]$ – HB morphology comparison between the LMC clusters and different GGC populations. In Figure 18, we plot our version of HB-type versus $[Fe/H]$ originally shown in Lee (1990). The O98 clusters at their revised metallicities show nice agreement with the inner halo clusters of the Galaxy, while our clusters fall among the outer halo clusters, as originally noted by Zinn (1993). Since the O98 clusters were not well-studied before HST and had no HB-type, they were not included in the analysis of Zinn (1993). However, with the new data, we can see that if the LMC contributes all of its GCs to the MW halo, it will contribute clusters like those in the inner halo as well, in about equal proportions.

There is another interesting, though tentative point. If we accept the O98 metallicities, then, as is the case for the GGC, the LMC clusters also separate into two groups in the HB-type versus $[Fe/H]$ plot. One group, composed of the O98 clusters, has higher $[Fe/H]$ ’s but not redder HBs than the other, which includes all the clusters studied by Walker (1992b), including NGC 1466, NGC 2257 and Hodge 11. The LMC groups also mimic the GGC in their spatial distribution differences. The O98 clusters are concentrated toward the center of the LMC. They all have projected angular separations $< 2.5^\circ$ from the LMC center, whereas the Walker sample has no clusters closer than 2.5° from the center. Based on our analysis in §6.2.1,

TABLE 10
 Δ AGES (GYRS) FOR COMPARISON GGCs

Source	M92	M55	M3	M5	Method
Richer <i>et al.</i> (1996)	0.0	0.5	-1.7	$\delta(V-I)$
Chaboyer <i>et al.</i> (1996b)	0.0	-2.6	-4.9	-4.3	ΔV
Gratton <i>et al.</i> (1997)	0.0	-2.9	MS fitting
Buonanno <i>et al.</i> (1998)	0.0	1.1	-0.2	-0.2	$\Delta V, \delta(V-I)$

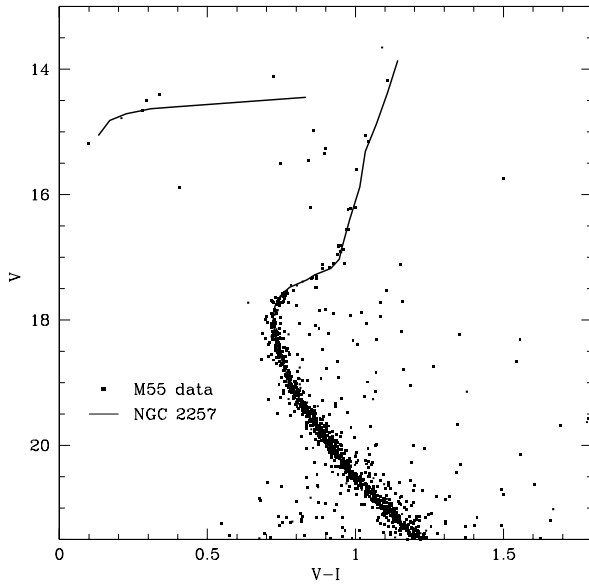


FIG. 17.— NGC 2257's fiducial compared to the M 55 data of Mandushev *et al.* (1996). The overall agreement between these two clusters of comparable metallicity shows that there is not a large age difference between them.

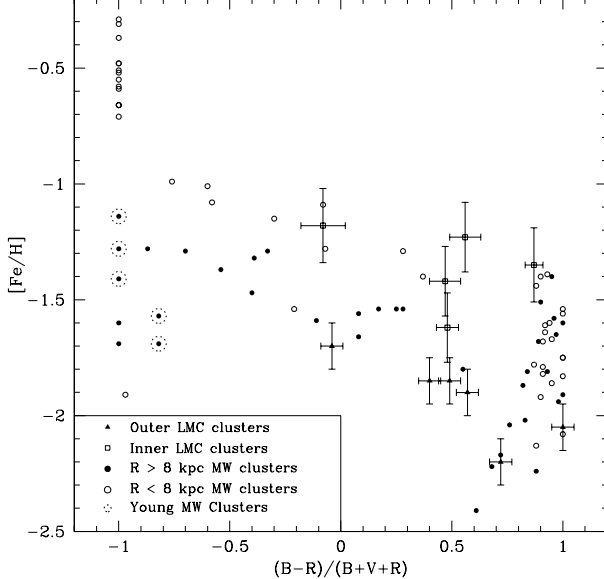


FIG. 18.— HB-type versus [Fe/H] for LMC and Galactic globular clusters. The HB-type is defined to be the number of blue stars minus the number of red stars divided by the total number of stars on the HB, including variables. The Galactic clusters have been divided into two groups, as suggested by Lee *et al.* (1994). Those MW clusters with $R < 8$ kpc tend to have bluer HBs than similar metallicity ones with $R > 8$ kpc. The LMC clusters display the same trend when the inner and outer clusters are compared. The data for inner LMC clusters are from Olsen *et al.* (1998), while the data for the outer ones are from Walker (1992b). The data for the MW come from the compilation in Lee *et al.* (1994). We have marked with a dotted circle those MW clusters that are most likely truly young clusters, based on their turnoff magnitudes. They are concentrated at even redder HBs than the LMC clusters.

where we discussed the age range among all the LMC clusters studied with HST, it is possible that age in this case is not the second parameter, a point also made by Da Costa (1999). A picture where the LMC builds up its outer GCs by accreting satellites is also less appealing, because of the mass of the LMC is not much larger than the mass of the smallest satellites known to have their own globular cluster systems. An additional clue to the formation of the LMC cluster system comes from the possible radial abundance gradient, if the O98 metalicities are correct (Da Costa 1999).

6.2.3. The Big Picture

Our most fundamental result is that the oldest LMC clusters are the same age as the old GGC. What does this mean for our understanding of galaxy formation? On one extreme, if we imagine the Galaxy being made completely via the accumulation of LMC-sized fragments (and if we accept the argument of Stetson *et al.* (1996) that most GGC are essentially coeval), then this coincidence in age would be telling us that the collapse epoch of all the original fragments was the same to 1.5 Gyr or so. In the opposite extreme, in which only a small fraction of the current-day Galaxy was acquired through accumulation of small companions, our result is then telling us that the formation epoch for the Milky Way out to the intermediate halo is the same to ~ 1.5 Gyr as for the LMC, a galaxy ten times less massive.

We discuss briefly here this result in the context of one (popular) galaxy formation scenario – hierarchical clustering (e.g., Blumenthal *et al.* 1984). It is not yet possible to fully simulate the processes that lead to galaxy formation. In particular, the question of when globular clusters form within hierarchical clustering models is not yet accessible to simulations. Nevertheless, with the reasonable assumptions that globular clusters were formed within larger structures (e.g. a proto-LMC) and

were among the first objects formed after the gas began to collapse, we can investigate whether the current hierarchical formation models can be consistent with our “fossil record” data. We note that as the models become more complete and sophisticated, this discussion may become rapidly dated. Nevertheless, as the data for globular cluster ages continue to improve, they will become increasingly important in testing models such as these.

As an example of what hierarchical clustering models predict for the formation epoch of LMC-like galaxies, we examined the properties of galaxies in 100 “Milky Way” halos calculated by the semi-analytic method of Somerville & Kolatt (1999) and Somerville & Primack (1999). These semi-analytic models are a powerful way to study galaxy formation by combining merging histories for dark-matter halos based on extended Press-Schechter theory (Bower 1991; Bond *et al.* 1991) with simple prescriptions for such physical processes as gas cooling, star formation and supernova feedback. The advantage of using this method is that the formation and evolution of many systems in many different cosmologies can be calculated in a reasonable period of time.

Placing GC formation in this scenario is difficult, because there is no agreed-on model of globular cluster formation and these models are not hydrodynamical calculations that can probe globular cluster formation. However, since the globular clusters are slightly metal-enriched and since models of globular cluster formation generally start with cold molecular gas (e.g., Harris and Pudritz 1994; Elmegreen & Efremov 1997), we can place the epoch of formation just after the gas can cool and start to form stars. When this happens depends on the mass of the dark matter halo. Because of the meta-galactic UV field, gas is prevented from cooling until its dark matter halo has reached the critical mass when its gas is dense enough to be self-shielded from ionizing photons. Simulations have shown

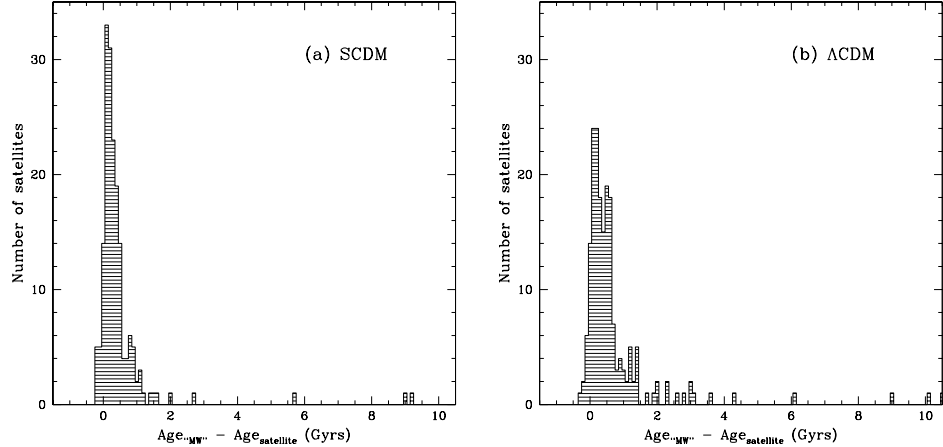


FIG. 19.— A histogram of the time lapse between the collapse of the first progenitor of the parent galaxy and of each of its bright ($M_B - 5\log \leq -15$) satellites for our “Milky Way” halos in (a) a standard CDM universe and (b) a Λ CDM universe. At the level that we can determine age differences, these two distributions are essentially the same.

that while this critical mass depends on redshift, it is not sensitive to such details as the shape of the UV-spectrum and the inclusion of star formation, especially at the level of precision we require (e.g., Weinberg, Hernquist & Katz 1997).

For each present-day galaxy in our “Milky Way” halo catalog, we have the redshift (z_{coll}) when any of the halos in that particular galaxy’s merging tree reached that critical mass in dark matter (the “first progenitor”). We assume that this marks the initial stage of globular cluster formation. We confine our results here to those satellites with $M_B < 5\log(h) - 15^2$, which includes the LMC and SMC, but not the dwarf spheroidals.

To illustrate the range of separation in time of this epoch, we calculated the difference in z_{coll} between the Milky-Way type galaxy and each of its satellites in the 100 model halos. The results are plotted in Figures 19a-b for two different cosmologies, standard cold dark matter (SCDM) with $\Omega_{matter} = 1.0$ and $H_0 = 50 \text{ km s}^{-1} \text{ Mpc}^{-1}$ and cold dark matter with a cosmological constant (Λ CDM) with $\Omega_\Lambda = 0.7$, $\Omega_{matter} = 0.3$, and $H_0 = 70 \text{ km s}^{-1} \text{ Mpc}^{-1}$. While there is a tail to large age differences, there is a strong peak at small age differences in both cosmologies. We cannot measure age differences much smaller than 1 Gyr. Therefore, if we assume that the initial epoch of globular cluster formation in a galaxy happened at about the same time as the collapse of the first progenitor of that galaxy, then our result that the oldest LMC and the Galactic clusters formed at the same time ± 1.5 Gyr is completely consistent with current hierarchical clustering models. As Harris *et al.* (1997) pointed out, this apparent synchronicity between the LMC and Galaxy, and within the outer halo of the Galaxy, is due to a number of *individual* dark matter halos approximately simultaneously reaching a critical mass so that star formation can start. The SMC provides a counter-example as it apparently began its cluster formation ~ 2 Gyr later (e.g., Stryker, Da Costa, & Mould 1985; Mighell, Sarajedini, & French 1998). In our hierarchical clustering models, it would be in the tail of the “Milky Way”-satellite age distribution.

We conclude that hierarchical clustering models, at least as described by current semi-analytical codes, are consistent with both constraints mentioned at the beginning of this section, though it is slightly harder to satisfy the first constraint for a

Λ CDM case. While many LMC-size galaxies form at about the same time, there is dispersion in z_{coll} , making it less likely to have all the original fragments collapse at the same time. On the other hand, the mass difference between the Milky Way and the LMC is not enough for it to be unusual for the collapse of the first progenitor to happen at the same time for both galaxies.

We would like to thank Dan Kelson, Raja Guhathakurta, Ata Sarajedini, and Eric Sandquist for useful suggestions and computer programs. Our thanks to V. Testa, A. Walker, K. Mighell, and G. Mandushev for providing their data on these clusters. J. A. J. acknowledges partial support from an NSF Graduate Student Fellowship. M. B. is happy to acknowledge support for this program from NASA grant GO-5897.01 administered through STScI and NSF grant AST 94-20204.

² $h = H_0/100$

REFERENCES

Andersen, J., Blecha, A., & Walker, M. F. 1984, MNRAS, 211, 695

Bergbusch, P. A. & VandenBerg, D. A. 1992, ApJS, 81, 163

Blumenthal, G. R., Faber, S. M., Primack, J. R., & Rees, M. J. 1984, Nature, 311, 517

Bolte, M., Hesser, J. E., & Stetson, P. B. 1993, ApJL, 408, L89

Bond, J. R., Cole, S., Efstathiou, G., & Kaiser, N. 1991, ApJ, 379, 440

Bower, R. 1991, MNRAS, 248, 332

Brocato, E., Castellani, Ferraro, F. R., Piersimoni, A. M., & Testa, V. 1996, MNRAS, 282, 614

Buonanno, R., Corsi, C. E., Pulone, L., Fusi Pecci, F., & Bellazzini, M. 1998, A&A 333, 505

Carretta, E. & Gratton, R. G. 1997, A&AS, 121, 95

Chaboyer, B., Demarque, P., Kernan, P. J., Krauss, L. M., & Sarajedini, A. 1996a, MNRAS, 283, 683

Chaboyer, B., Demarque, P. & Sarajedini, A. 1996b, ApJ, 459, 558

Chaboyer, B. & Kim, Y.-C. 1995, ApJ, 454, 767

Cohen, R. L., Guhathakurta, P., Yanny, B., Schneider, D. P., & Bahcall, J. N. 1997, AJ, 113, 669

Cowley, A. P. & Hartwick, F. D. A. 1982, ApJ, 259, 89

Cool, A. M. & King, I. R. 1995 in Calibrating Hubble Space Telescope: Post Servicing Mission, ed. A. Koratkar & C. Leitherer (Baltimore: STScI), 290

Da Costa, G. S. 1999 in New Views of the Magellanic Clouds, IAU 190, ed. Y-H. Chu, N. Suntzeff, J. Hesser, & D. Bohlender, in preparation

Da Costa, G. S. & Armandroff, T. E. 1990, AJ, 100, 162

Elmegreen, B. G. & Efremov, Y. N. 1997, ApJ, 480, 235

Feast, M. W. & Catchpole, R. M. 1997, MNRAS, 286, L1

Fernley, J., Barnes, T. G., Skillen, I., Hawley, S. L., Hanley, C. J., Evans, D. W., Solano, E., & Garrido, R. 1998, 330, 515

Frenk, C. S. & Fall, S. M. 1982, MNRAS, 199, 565

Goodwin, S. P. 1997, MNRAS, 286, 39

Gould, A. & Uza, O. 1998, ApJ, 494, 118

Gratton, R. G., Fusi Pecci, F., Carretta, E., Clementini, G., Corsi, C., & Lattanzi, M. 1997, ApJ, 491, 749

Guhathakurta, P., Yanny, B., Bahcall, J. N., & Schneider, D. P. 1994, AJ, 108, 1786

Guhathakurta, P., Yanny, B., Schneider, D. P., & Bahcall, J. N. 1992, AJ, 104, 1790

Harris, W. E. 1996, AJ, 112, 1487

Harris, W. E., Bell, R. A., VandenBerg, D. A., Bolte, M., Stetson, P. B., Hesser, J. E., van den Bergh, S., Bond, H. E., Fahlman, G. G., & Richer, H. B. 1997, AJ, 114, 1030

Harris, W. E. & Pudritz, R. E. 1994, ApJ, 429, 177

Hesser, J. E., McClure, R. D., & Harris, W. E. 1984, in Structure and Evolution of the Magellanic Clouds, IAU 108, ed. S. van den Bergh & K. S. de Boer (Dordrecht: D. Reidel Publishing Co.), 47

Holtzman, J. A., Burrows, C. J., Casertano, S., Hester, J. J., Trauger, J. T., Watson, A. M., & Worthey, G. 1995, PASP, 107, 1065

Johnson, J. A. & Bolte, M. 1998, AJ, 115, 693

Krist, J. 1995, in Astronomical Data Analysis Software and Systems IV, ASP Conference Series 77, ed. R. A. Shaw, H. E. Payne, & Hayes, J. J. E. (San Francisco: Astronomical Society of the Pacific), 349

Langer, G. E., Bolte, M., & Sandquist, E. 1999, ApJ, in press

Lee, Y.-W. 1990, ApJ, 363, 159

Lee, Y.-W., Demarque, P., & Zinn, R. 1994, ApJ, 423, 248

Mandushev, G. I., Fahlman, G. G., Richer, H. B., & Thompson, I. B. 1996, AJ, 112, 1536

Mateo, M. 1987, ApJL, 323, L41

Mighell, K. J., Rich, R. M., Shara, M., & Fall, S. M. 1996, AJ, 111, 2314

Mighell, K. J., Sarajedini, A., & French, R. S. 1998, AJ, 116, 239

Nemec, J. M. & Cohen, J. G. 1989, 336, 780

Pont, F., Mayor, M., Turon, C., & VandenBerg, D. A. 1998, A&A, 329, 87

Olsen, K. A. G., Hodge, P. W., Mateo, M., Olszewski, E. W., Schommer, R. A., Suntzeff, N. B., & Walker, A. R. 1998, MNRAS, 300, 665

Olszewski, E. W., Schommer, R. A., Suntzeff, N. B., & Harris, H. C. 1991, AJ, 101, 515

Richer, H. B., Harris, W. E., Fahlman, G. G., Bell, R. A., Bond, H. E., Hesser, J. E., Holland, S., Pryor, C., Stetson, P. B., VandenBerg, D. A., & van den Bergh, S. 1996, ApJ, 463, 602

Rutledge, G. A., Hesser, J. E., & Stetson, P. B. 1997, PASP, 109, 907

Salaris, M., Chieffi, A., & Straniero, O. 1993, ApJ, 414, 580

Sandage, A. R. 1982, ApJ, 252, 553

Sandage, A. R. & Smith, L. L. 1966, ApJ, 144, 886

Sandquist, E., Bolte, M., Stetson, P. B., & Hesser, J. E. 1996, ApJ, 470, 910

Sarajedini, A., Chaboyer, B., & Demarque, P. 1997, PASP, 109, 1321

Sarajedini, A. & Demarque, P. 1990, ApJ, 365, 219

Schommer, R. A., Suntzeff, N. B., Olszewski, E. W., & Harris, H. C. 1992, AJ, 103, 447

Searle, L. & Zinn, R. J. 1978, ApJ, 225, 357

Somerville, R. S. & Kolatt, T. S. 1999, MNRAS, 305, 1

Somerville, R. S. & Primack, J. R. 1999, MNRAS, in press (astro-ph/9802268)

Sosin, C. & King, I. R. 1995, AJ, 109, 639

Stanek, K. Z., Zaritsky, D., & Harris, J. 1998, ApJ, 500, L141

Stetson, P. B. 1987, PASP, 99, 191

Stetson, P. B. 1992, JRASC, 86, 71

Stetson, P. B. 1993, in Stellar Photometry—Current Techniques and Future Developments, IAU 136, ed. C. J. Butler & I. Elliot (Cambridge University Press, Cambridge), p. 291

Stetson, P. B. 1994, PASP, 106, 250

Stetson, P. B. 1998, PASP, 110, 1448

Stetson, P. B., *et al.* 1999, AJ, 117, 247

Stetson, P. B., VandenBerg, D. A., & Bolte, M. 1996, PASP, 108, 560

Stryker, L. L. 1983, ApJ, 266, 82

Stryker, L. L., Da Costa, G. S., & Mould, J. R. 1985, ApJ, 298, 544

Stryker, L. L., Nemec, J. M., Hesser, J. E., & McClure, R. D. 1984, in Structure and Evolution of the Magellanic Clouds, IAU 108, ed. S. van den Bergh & K. S. de Boer (Dordrecht: D. Reidel Publishing Co.), 43

Suntzeff, N. B., Schommer, R. A., Olszewski, E. W. & Walker, A. R. 1992, AJ, 104, 1743

Sweigart, A. V. 1997, ApJ, 474, L23

Testa, V., Ferraro, F. R., Brocato, E., & Castellani, V. 1995, MNRAS, 275, 454

Trager, S. C., King, I. R., & Djorgovski, S. 1995, AJ, 109, 218

van den Bergh, S. 1967, AJ, 72, 70

van den Bergh, S. 1995, ApJ, 451, L65

van den Bergh, S. 1996, PASP, 108, 986

van den Bergh, S. & Morbey, C. L. 1984, ApJ, 283, 598

VandenBerg, D. A., Bolte, M., & Stetson, P. B. 1990, AJ, 100, 445 (VBS)

Walker, A. R. 1989, AJ, 98, 2086

Walker, A. R. 1992a, ApJL, 390, L81

Walker, A. R. 1992b, AJ, 104, 1395

Walker, A. R. 1993, AJ, 106, 999

Webbink, R. F. 1985, in Dynamics of Star Clusters, IAU 113, ed. J. Goodman & P. Hut (Dordrecht: D. Reidel Publishing Co.), 541

Weinberg, D. H., Hernquist, L., & Katz, N. 1997, 477, 8

Westerlund, B. E. 1997, The Magellanic Clouds, (Cambridge: Cambridge University Press)

Whitmore, B. & Heyer, I. 1997, Instrument Science Report WFPC2 97-08

Yanny, B., Guhathakurta, P., Schneider, D. P., & Bahcall, J. N. 1994, 435, L59

Zinn, R. 1980a, ApJS, 42, 19

Zinn, R. 1980b, ApJ, 241, 602

Zinn, R. 1993, in The Globular Cluster-Galaxy Connection, ASP conference Series 48, ed. G. H. Smith & J. P. Brodie (San Francisco: ASP), 302

Zinn, R. & West, M. J. 1984, ApJS, 55, 45